Available online at www.sciencedirect.com
ScienceDirect
Nuclear Instruments and Methods in Physics Research A 586 (2008) 239–245
NUCLEAR INSTRUMENTS & METHODS IN PHYSICS RESEARCH Section A
www.elsevier.com/locate/nima

Proton and neutron production from GAMMA-2 spallation source irradiated by relativistic proton beams

M. Manolopoulou[a,*], S. Stoulos[a], M. Fragopoulou[a], R. Brandt[b], W. Westmeier[b], M.I. Krivopustov[c], N.A. Sosnin[c], S.R. Hashemi-Nezhad[d], M. Zamani-Valasiadou[a]

[a]*Physics Department, Aristotle University of Thessaloniki, 541 24 Thessaloniki, Hellas*
[b]*Philipps Universität, 35032 Marburg, Germany*
[c]*Joint Institute for Nuclear Research, 141980 Dubna, Russia*
[d]*School of Physics, A28, University of Sydney, NSW 2006, Australia*

Received 2 April 2007; received in revised form 24 October 2007; accepted 22 November 2007
Available online 26 December 2007

Abstract

In the frame of international concern about long-lived nuclear waste, the construction of an effective accelerator driven system for the transmutation or incineration of fission products and actinides is a promising task. A spallation source consisting of a Pb target surrounded by paraffin moderator was studied by irradiation with relativistic proton beams. The spatial distribution of secondary proton and slow neutron were determined using the ^{nat}Cd activation technique and their multiplicity was calculated in order to verify the transmutation efficiency of the specific spallation source and to estimate the tolerance limit of source construction materials.

PACS: 25.40.S; 29.25.D; 29.40.Y; 82.80.J

Keywords: Proton and neutron distribution; Spallation sources; Transmutation

1. Introduction

An accelerator driven system (ADS) whereas a high intensity ion beam hitting a spallation source could well compete a high flux reactor in terms of neutron production in order to transmute long-lived nuclear waste and/or to produce energy [1–3]. A detailed engineering design of an ADS spallation source requires an optimization of its performance in terms of neutron production, and an assessment of problems occurring in such systems. The number of spallation neutrons produced per incident particle in various target materials and in different geometries as well as the energy spectrum and angular distribution of spallation neutrons must be known in order to optimize the design of the source. In particular, the shape of the neutron spectrum is a decisive factor for the source efficiency regarding its use for transmutation or incineration purposes. During the spallation process, in addition to neutron production, a large amount of secondary charged hadrons, mainly protons, and many gamma rays are also emitted from the target. In order to cope with the intense radiation field around a spallation source, an effective shielding to energetic hadrons and photons is required. The structural materials of the source have to be chosen so as to tolerate not only fast secondary neutrons but also the secondary protons as well as protons generated by (n,xp) or (p,xp) reactions and slowed down inside the material [4]. Especially, secondary protons are of high interest regarding the possibility of additional channels for transmutation or incineration by proton-induced reactions.

During the last decades, several spallation sources for solid-state and material physics have been constructed and studied worldwide. Many experimental results as well as Monte Carlo calculations about spallation physics and neutron multiplicity have been presented [5–10]. In addition, various spallation sources for transmutation or

*Corresponding author. Tel.: +30 2310 998217; fax: +30 2310 998176.
E-mail address: metaxia@auth.gr (M. Manolopoulou).

0168-9002/$ - see front matter © 2007 Elsevier B.V. All rights reserved.
doi:10.1016/j.nima.2007.11.043

incineration experiments have already been tested and they need continued consideration [11–14]. Among these is the GAMMA-2 set-up, a Pb target surrounded by a 6-cm-thick paraffin moderator, which is built with the intention to study transmutation via neutron capture and neutron-induced fission. The ^{239}Pu(n,f), ^{238}U(n,γ), ^{237}Np(n,γ), ^{129}I(n,γ) transmutation effectiveness has been studied in irradiations using relativistic proton beams [17,18,23]. Moreover, the neutron distribution along the target and moderator has been determined using various passive methods [15–23] measuring the wide energy range of emitted neutrons. However, no experimental data of the secondary proton distribution has been presented until now.

In the present work, the spatial distribution of secondary protons along the moderator is presented which can be used to evaluate the tolerance of structural materials in source design and construction. The secondary proton distribution was determined using ^{nat}Cd activation techniques [24]. In addition, using the same activation detector, the distribution of secondary slow neutrons was also determined. Their spatial distribution along the moderator is presented in order to estimate the slow neutron multiplicity that is a measure of the transmutation efficiency of the source.

2. Experimental

The GAMMA-2 transmutation set-up is a spallation source with a cylindrical lead target 8 cm in diameter and 20 cm in length covered by a paraffin moderator of 6 cm thickness (Fig. 1). The target was irradiated with 0.65, 1 and 3.7 GeV proton beams and slow neutrons fluencies were determined along the moderator. Moreover, an extended GAMMA-2 set-up, with a lead target 40 cm in length, was irradiated with 1, 1.5 and 2 GeV proton beams and slow neutron and secondary proton was measured. Irradiations were performed at the Nuclotron accelerator in the High Energy Laboratory of JINR in Dubna (Russia).

Natural Cd foils of 1 mm thickness (mass approximately 2 g, purity 99.9%) were placed along the paraffin moderator, parallel to the cylinder axis (Fig. 1). These samples were used to measure the slow neutron as well as secondary proton fluencies. The calculation and measuring method were described in detail elsewhere [24]. The natural Cd foil effectively captures neutrons below 1 eV, mainly because of

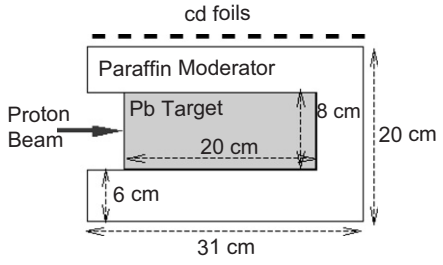

Fig. 1. The GAMMA-2 (Pb/paraffin target) set-up.

the very high cross section of ^{113}Cd for thermal neutron capture. Epithermal neutron fluence was determined from the concentrations of ^{115}Cd and its daughter ^{115}In, produced via ^{114}Cd(n,γ)^{115}Cd. The effective cross section for the ^{114}Cd(n,γ)^{115}Cd reaction at the resonance area can be calculated as follows:

$$\sigma_{\mathrm{eff}}(\mathrm{n},\gamma) = \frac{\int_{1\,\mathrm{eV}}^{10000\,\mathrm{eV}} \sigma_{(n,\gamma)}(E)(\mathrm{d}E/E)}{\int_{1\,\mathrm{eV}}^{10000\,\mathrm{eV}} (\mathrm{d}E/E)} = \frac{\text{Resonance Integral}}{\ln(10000)} = \frac{13\pm 2}{9.21} = 1.41\pm 0.22b \tag{1}$$

where $\sigma(E)$ is the excitation function of the relevant reaction and neutron fluence is described by the $1/E$ function at the resonance area (1 eV up to 10 keV). The Resonance Integral was taken $13\pm 2b$, as it is defined at the NuDat 2.4 file (www.nndc.bnl.gov/nudat2) However, significant number of epithermal neutrons reacts with other cadmium isotopes, as natural Cd has eight stable isotopes. To cope with the influence of other isotopes as well as the self-shielding effect due to the sample thickness, a Monte Carlo simulation was performed with GEANT4 [26]. The number of Cd isotopes nuclei produced from all possible reactions per neutron hitting the surface of the sample was thus calculated. Neutron kinetic energy was defined in isolethargic steps for the energy region from thermal up to 20 MeV. The results of GEANT4 calculations for every energy step in the form of (cadmium isotope nuclei produced)/(neutron hitting the surface of the sample) were coupled with neutron spectrum on the surface of paraffin moderator (see Fig. 2) which is calculated also by Monte Carlo simulations with the codes MCNPX and DCM-DEC [19,25]. From these calculations it is deduced that $74.2\pm 2.5\%$ of ^{115}Cd nuclei originated from epithermal neutrons (1 eV up to 10 keV) with an effective cross section $1.15\pm 0.03b$ for ^{114}Cd(n,γ)^{115}Cd reaction. The uncertainty refers only to the statistical accuracy of the calculations. Including the cross section data uncertainties, the effective cross section becomes $1.15\pm 0.18b$. This value is somehow smaller than the calculated from Eq. (1) due to the self-shielding effect because of the sample thickness.

Natural Cd has a significant cross section to the ^{nat}Cd(p,x)^{111}In reaction as it is reported in Ref. [27], in the energy range $1\,\mathrm{MeV}\leqslant E_{\mathrm{p}}\leqslant 100\,\mathrm{MeV}$ which covers well the secondary proton spectrum around the GAMMA-2 target (Fig. 2). In order to take into account the energy loss of protons in Cd sample due to the sample thickness (1 mm) the Continuous Slow Down Approximation method with data provided by ICRU94 [28] was applied (Fig. 3). The determined effective cross section is $0.14\pm 0.02b$ for proton energy range 1–100 MeV.

The Cd foils were measured several times over two weeks using a low-level HPGe γ-ray spectrometry system. The system consists of a coaxial detector with 42% relative efficiency, 2.2 keV resolution for 1.33 MeV photons (^{60}Co) and shielded by 4 in. low-background Pb with an inner

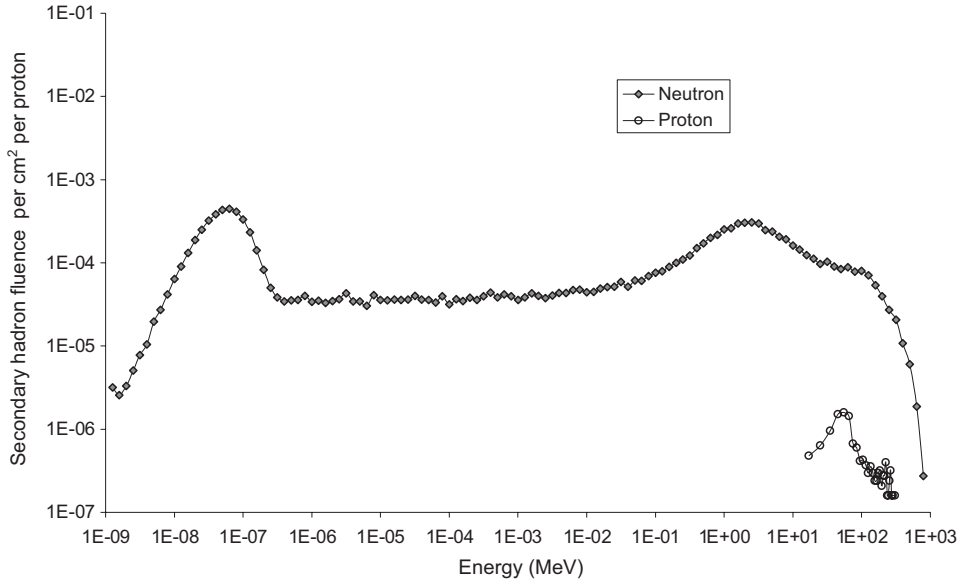

Fig. 2. The energy dependent secondary hadron fluence calculated on the surface of the paraffin moderator by using Monte Carlo simulations for 1 GeV incoming proton beam.

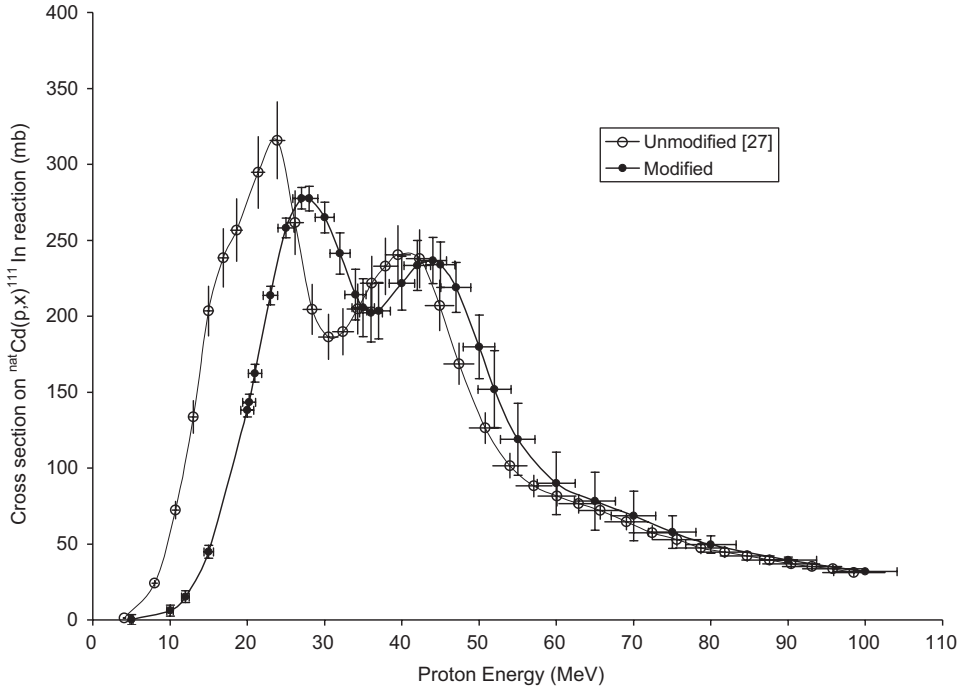

Fig. 3. Excitation function data for $^{nat}Cd(p,x)^{111}In$ reaction before [27] and after modification for proton energy loss in Cd foil.

lining of 1 mm Cd and 1 mm Cu, a high voltage power supply, an amplifier with pile-up rejector and a computer based multichannel analyzer. The quantification of ^{115}Cd was made over decay curves of the two most intense γ-rays at 336 and 528 keV. The ^{111}In was determined using the decay curves of 171 and 245 keV γ-rays, with consideration of the essential correction factors for summation effect that were calculated for the specific sample geometry.

The hadron fluence per cm^2 and per incoming proton was derived from the gamma activity measurements (C, counts) using the following equation:

$$\Phi = \frac{C \times f_\gamma}{f_{\text{decay}} \times f_{\text{beam}} \times \varepsilon \times I_\gamma} \frac{f_b}{\sigma_{\text{eff}} \times N \times F_p} \tag{2}$$

where f_γ is the self-attenuation correction factor for the measured γ-rays that ranged from 4% up to 16% for gamma ray energy of 528 keV down to 171 keV, $f_{\text{decay}} = (1 - e^{-\lambda t_m}) e^{-\lambda t_a}$ corresponds to the decay process during the measurement (t_m) and the waiting time (t_a)

between the end of irradiation and the begging of the measurement, λ is the decay constant. The $f_{\text{beam}} = (1 - e^{-\lambda t_{\text{ir}}}/\lambda t_{\text{ir}})$ correction factor corresponds to the decay process during the irradiation time (t_{ir}) for the monitoring isotope, which has a half-life much longer than the beam breaks. The factors ε is the counting efficiency, I_γ is the γ-ray fraction corrected for summation effect, σ_{eff} the experimental effective cross section and N the foil nuclei. The f_b stands for beam asymmetry correction and it ranged from 1% up to 12% and F_p is the integrated proton fluence measured using the standard Al monitoring technique [22]. The uncertainties contribution to fluence measurement is presented in details in Table 1.

3. Results and discussion

3.1. Neutron spatial distribution

The spatial distribution of epithermal neutrons measured along the paraffin moderator in irradiations with a 1 GeV proton beam for both GAMMA-2 set-ups are presented in Fig. 4. In the same figure data obtained during a previous irradiation of the 20 cm Pb target with a 1 GeV proton beam [24], evaluated using the effective cross section that determined at the present work, are also presented. The maximum at $1.4 \pm 0.3 \times 10^{-3}$ epithermal neutrons cm^{-2} per incoming proton is found at about 15 cm along the moderator, corresponding to about 10 cm along the Pb target, independently of the target length. Although the maximum intensity of neutrons is found at the same location (5 cm up to 15 cm along the Pb target) on both set-ups, their spatial distribution along the target is somehow different. The extension of the Pb target from 20 to 40 cm length provides additional target material for neutron production, which is actually used because the range for 1 GeV protons in Pb is 55 cm. Thus, a neutron increment is observed at the extended target beyond 15 cm along the Pb target (see Fig. 4). The neutron increment at the entrance of the extended Pb target might be attributed to back-scattered neutrons produced further along the target.

Table 1
The uncertainties contribution over the hadron fluence determination

Source of uncertainty	Neutron	Proton
Foil mass (%)	<0.1	<0.1
Counting statistics (%)	<2	4–8
Beam intensity (%)	6–10	6–10
Ge efficiency × γ-fraction (%)	~3	~3
Effective cross section σ_{eff} (%)	16	14
Total (%)	17–19	16–19

The neutron and proton distribution over the paraffin surface reflects the hadron production in the Pb target from spallation reactions induced by primary and secondary particles as well as their moderation and attenuation in the paraffin. The experimental spatial distribution of hadrons can be explained by taking into account the interactions of high-energy protons in a thick target where two competitive effects have to be considered: an exponential increase of secondary particle production in the beginning of the target (build-up effect) and an exponential decrease of the intensity of the primary proton beam along the target (attenuation effect) [8]. A fitting procedure was applied to the neutron fluence ρ_n (in units of neutrons cm^{-2} proton^{-1}) as a function of the beam path x in cm along the target using the equation [29]:

$$\rho_n = C(1 - \alpha e^{-bx}) e^{-dx}. \quad (3)$$

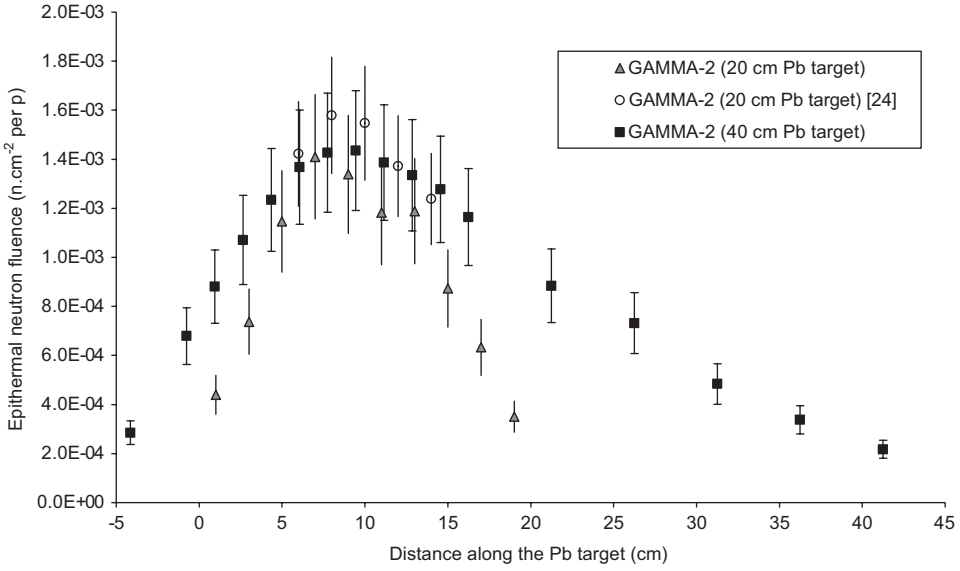

Fig. 4. Spatial distributions of epithermal neutrons measured along the paraffin moderator in irradiations with 1 GeV proton beam of both GAMMA-2 set-ups. The lines appeared is to guide the eye.

The neutron spatial distribution measured during irradiations of the extended GAMMA-2 target is presented in Fig. 5. The neutron production in the Pb target is going up with proton beam energy increment. The maximum of the epithermal neutron density is measured to be independent of target length at 10 ± 1 cm from the beam entrance into the target for all proton energies studied, which approximates the mean free path of primary protons in Pb. The fitted attenuation coefficient $d = 0.060 \pm 0.009\,\mathrm{cm}^{-1}$ is shown to be independent of proton beam energy. This experimental value corresponds well to the known interaction length $\lambda \approx 1/d \approx 17$ cm for 1–2 GeV protons in Pb. Results fitted to data measured on the 20 cm Pb target GAMMA-2 set-up appear to be similar to those obtained from the thermal and fast neutron spatial distribution determined during the same irradiations using solid-state nuclear track detectors [29].

3.2. Proton spatial distribution

Applying the above fitting procedure to the secondary proton spatial distribution (Fig. 6) the attenuation coefficient d is also shown to be independent of proton beam energy with a mean value $d = 0.055 \pm 0.007\,\mathrm{cm}^{-1}$, identical within 1σ uncertainty to the value obtained for the neutron distribution. The maximum fluence of secondary

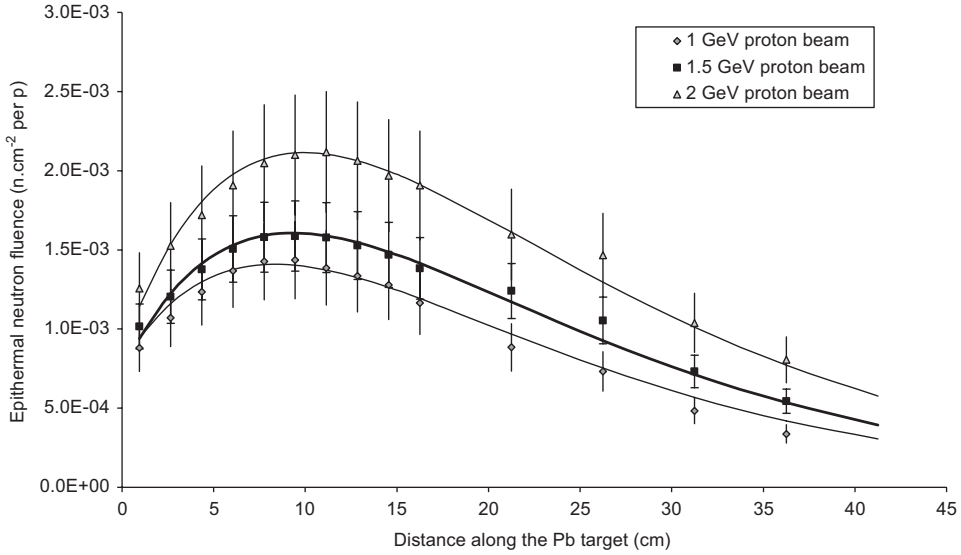

Fig. 5. Spatial distributions of epithermal neutrons measured along the paraffin moderator in irradiations of the extended GAMMA-2 set-up with proton beams of different energies. The lines represent the fitting function (Eq. (2)) applied to the data points.

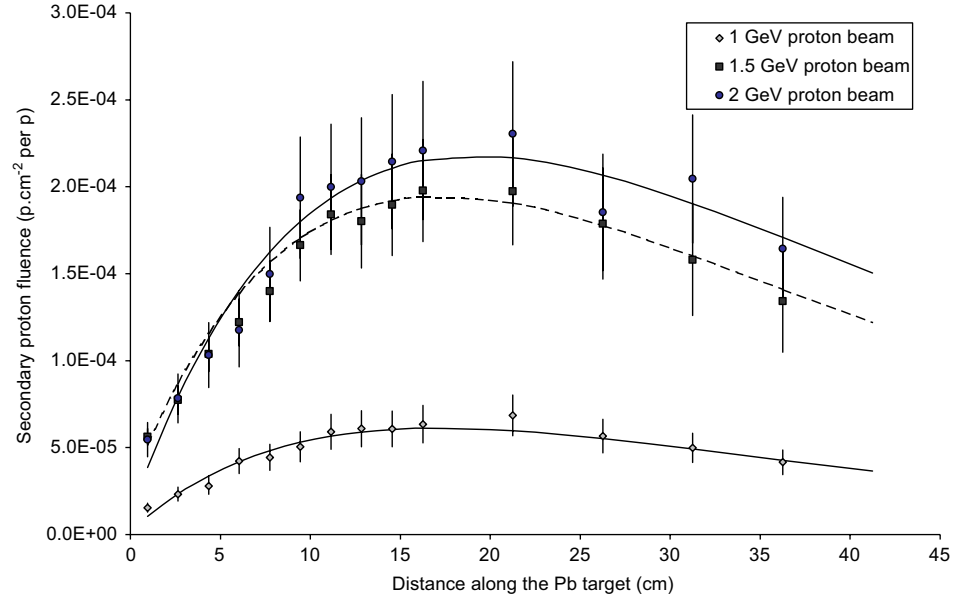

Fig. 6. Spatial distributions of secondary protons measured along the paraffin moderator during irradiations of extended GAMMA-2 set-up with proton beams of different energies. The lines represent the fitting function (Eq. (2)) applied to the data points.

protons for all primary proton beam energies, however, is found at 17 ± 2 cm from beam entrance into the target, which is distinctly different from 10 ± 1 cm measured for neutrons. The secondary proton production in the Pb target appears to increase with rising proton beam energy but in a different way as compared to the production of neutrons. Comparing the proton fluence with the epithermal neutron fluence for the same incoming proton beam energy is evident that the proton density varies significantly less than that of epithermal neutrons.

To compare the total neutron with the secondary proton production, the entire neutron energy spectrum should be considered. The neutron spectrum released from the GAMMA-2 set-up extents up to several hundred MeV according to Monte Carlo calculations with DCM-DEC, LAHET and MCNPX codes [17,19,25]. Moreover, using solid-state nuclear track detectors it resulted in a considerable high number of thermal (up to 1 eV) and intermediate-fast (above 0.3 MeV) neutrons accompanying the epithermal (1 eV up to 10 keV) ones emitted from the specific set-up [21]. Taking into account the wide energy range of the neutron spectrum, the total number of neutrons produced during the spallation process in the GAMMA-2 set-up is about two orders of magnitude higher than that of secondary protons.

3.3. Neutron and proton production

In order to determine the neutron and proton multiplicity as a function of proton beam energy, the fitting function (Eq. (3)) was integrated over the entire cylindrical surface of the paraffin for both GAMMA-2 set-ups. Both epithermal neutron and secondary proton production increases continuously with proton beam energy (Table 2). Moreover, when the Pb target length is extended from 20 to 40 cm almost twice the number of secondary epithermal neutrons is produced for the same proton beam energy of 1 GeV. Using that neutron source in a hypothetical ADS with 10 mA proton beam, a considerable production rate of slow neutrons of 10^{17} neutrons s^{-1} will result in a substantial transmutation or incineration rate through (n,γ) or (n,f) reactions to long-lived fission products and actinides produced during the fuel process [18,23]. The operation of the ADS may require a proper moderator in order to slow down the secondary neutrons, particularly those emitted in intermediate-fast energy range (between 0.3 and 3 MeV), to energies useful for transmutation reactions. In addition, the released secondary protons rate 10^{16} protons s^{-1} has to be considered regarding to choose the appropriate constructing materials that should tolerate maximum 0.001 mol of hydrogen per day, assuming that the total amount of produced protons are trapped in the constructing materials of the source. Especially, the Pb target could be affected by one order of magnitude more hydrogen moles per day, noticing that the evaporating secondary protons are trapped in the target. So, the use of a liquid target could solve the problem since it is easier to remove the produced hydrogen and to avoid any adverse effects like bubbles or even cracks in the solid matter, as has been proposed by Bauer [8].

Table 2
Neutron and proton multiplicities determined in irradiations of both GAMMA-2 set-ups with relativistic proton beams

Proton beam energy (GeV)	Epithermal neutrons per primary proton		Secondary protons per primary proton
	20 cm Pb target	40 cm Pb target	40 cm Pb target
0.65	0.56 ± 0.09		
1	0.94 ± 0.16	1.76 ± 0.30	0.13 ± 0.02
1.5		2.05 ± 0.39	0.39 ± 0.07
2		2.79 ± 0.50	0.45 ± 0.08
3.7	1.65 ± 0.31		

4. Conclusions

Spallation neutron and proton distributions over the surface of GAMMA-2 set-up (a Pb target surrounded by paraffin moderator) were determined using ^{nat}Cd activation detector during irradiations with relativistic proton beams with kinetic energies 0.65–3.7 GeV. For all studied proton energies and independently of the Pb target length, the maximum neutron density is found at about 10 cm from the beam entrance into the target while the maximum proton density at 17 ± 2 cm. Secondary neutron and proton production increases with incoming proton beam energy increment. The total neutron production is about two orders of magnitude higher than the secondary proton.

Using this spallation target in a hypothetical ADS with 10 mA proton beam, the production rate of slow neutrons 10^{17} neutrons s^{-1} would cause substantial transmutation and incineration of long-lived fission products and actinides through (n,γ) or (n,f) reactions, where the latter might even be useful for energy production. That ADS requires proper moderation facility in order to reduce the energy of neutrons emitted in intermediate-fast energy range. Taking into account the secondary proton production rate of 10^{16} protons s^{-1}, the construction materials should be able to withstand up to 0.001 mol of hydrogen per day. The Pb target would be particularly affected by higher hydrogen implantation, thus the use of a liquid target could solve that problem.

Acknowledgments

The authors are grateful to Professor A.I. Malakhov and the staff of the Laboratory of High Energies, JINR Dubna, for their continuous support to our work. Special gratitude is due to Professor A.D. Kovalenko and the operation staff of the Nuclotron accelerator for providing stable high intensity beams during irradiations.

References

[1] C.D. Bowman, et al., Nucl. Instr. and Meth. Phys. Res. A 320 (1992) 336.
[2] F. Carminati, et al., Report CERN/AT/93-47 (ET), 1993.
[3] S. Andriamonje, et al., Phys. Lett. B 348 (1995) 697.
[4] A. Sinha, Nucl. Instr. and Meth. Phys. Res. A 274 (1989) 563.
[5] D. Hilscher, et al., Nucl. Instr. and Meth. Phys. Res. A 414 (1998) 100.
[6] J.M. Carpenter, et al., Physica B 270 (1999) 272.
[7] A. Letourneau, et al., Nucl. Instr. and Meth. Phys. Res. B 170 (2000) 299.
[8] G.S. Bauer, Nucl. Instr. and Meth. Phys. Res. A 463 (2001) 505.
[9] S. Leray, et al., Phys. Rev. C 65 (2002) 044621.
[10] K. van der Meer, et al., Nucl. Instr. and Meth. Phys. Res. B 217 (2004) 202.
[11] M. Ochs, et al., Radiat. Meas. 28 (1997) 255.
[12] TARC Collaboration, EUR19117, ISBN 92-828-7759-0 (1999).
[13] R. Brandt, et al., Radiat. Meas. 31 (1999) 497.
[14] M.I. Krivopustov, et al., Kerntechnik 68 (2003) 48.
[15] J.C. Adloff, et al., Radiat. Meas. 31 (1999) 551.
[16] S.R. Hashemi-Nezhad, et al., Radiat. Meas. 31 (1999) 537.
[17] J.S. Wan, et al., Nucl. Instr. and Meth. Phys. Res. A 463 (2001) 634.
[18] J. Adam, et al., Radiochim. Acta 90 (2002) 431.
[19] S.R. Hashemi-Nezhad, et al., Nucl. Instr. and Meth. Phys. Res. A 493 (2002) 121.
[20] R. Brandt, et al., Kerntechnik 69 (2004) 37.
[21] M. Zamani, et al., Radiat. Meas. 40 (2004) 410.
[22] W. Westmeier, et al., Radiochim. Acta 93 (2005) 65.
[23] J. Adam, et al., Nucl. Instr. and Meth. Phys. Res. A 562 (2006) 741.
[24] M. Manolopoulou, et al., Appl. Radiat. Isot. 64 (2006) 823.
[25] A.N. Sosnin, et al., Izvestiya RAS, Phys. Ser. 66 (2002) 1494.
[26] S. Aggostinelli, et al., Nucl. Instr. and Meth. Phys. Res. A 506 (2003) 250.
[27] F.M. Nortier, et al., Appl. Radiat. Isot. 41 (1990) 1201.
[28] ICRU Report 49, 1993.
[29] M. Fragopoulou, et al., Nucl. Instr. and Meth. Phys. Res. A 560 (2006) 571.